Received: 30 June 2020 | Revised: 24 October 2020 | Accepted: 2 November 2020 | Published on: 16 November 2020

DOI: 10.1002/joc.6923

RESEARCH ARTICLE

International Journal of Climatology RMetS

Historical trends of seasonal Greenland blocking under different blocking metrics

Lori J. Wachowicz[1] | **Jonathon R. Preece**[1] | **Thomas L. Mote**[1] | **Bradford S. Barrett**[2] | **Gina R. Henderson**[2]

[1]Department of Geography, University of Georgia, Athens, Georgia

[2]Oceanography Department, United States Naval Academy, Annapolis, Maryland

Correspondence
Lori J. Wachowicz, Department of Geography, University of Georgia, Athens, GA.
Email: lori.wachowicz@uga.edu

Funding information
NSF Arctic Systems Science, Grant/Award Number: 1900324; SERDP, Grant/Award Number: RC18-1658; Strategic Environmental Research and Development Program, Grant/Award Number: RC18-1658

Abstract

As the Arctic continues to warm, a weakening of upper-tropospheric westerly winds is hypothesized to induce a meandering jet stream and slower propagation of Rossby waves. As such, current hypotheses suggest an increase in Greenland blocking due to increased stationarity of the high amplitude waves. These hypotheses have been supported observationally with the Greenland blocking index (GBI). However, given an expected increase in overall geopotential heights corresponding to increased temperatures in the region, we assess the robustness of trends in Greenland blocking using additional blocking metrics in addition to the GBI, which has largely been the focused blocking metric for this region to date. Our results show sensitivity of the GBI-based increases in blocking to global and zonally averaged 500-hPa geopotential heights, which results in inconsistent increasing trends over the 1979–2018 period when compared with other blocking metrics. Seasonal blocking frequencies of the GBI show a significant increase in blocking for JJA, though no significant trend in JJA blocking occurs for most metrics. Other indices suggest a decrease in blocking frequency in September–November (SON) and December–February (DJF), though these trends are not statistically significant. Yet, when smoothed using a 5-year running mean, these other metrics suggest an increase in both DJF and JJA blocking with a decrease only in SON blocking, which are consistent with findings of significant changes in GBI. We report no best metric for identifying Greenland blocking. Instead, we present some shortcomings of the different metrics used in this study. These results provide insight into selection of Greenland blocking events for future research, as over- or under-estimation of blocking activity can impact estimates of surface mass balance of the ice sheet.

KEYWORDS

blocking, GBI, Greenland, trends

1 | INTRODUCTION

The Arctic is a region of rapid warming, partly due to a variety of feedbacks within the Earth system through a process known as Arctic amplification (Serreze and Francis, 2006; Dai *et al*., 2019). Recent work has found that this warming has led to a weakening of the zonal winds and a waiver, higher-amplitude jet stream, and in turn has resulted in the slower propagation of Rossby waves (Francis and Vavrus, 2012, 2015; Luo *et al*., 2018). Barotropic mechanisms, such as those associated with Rossby wave breaking, may act to decrease the speed and vary the position of the eddy-driven jet (Barnes *et al*., 2010; Ronalds *et al*., 2018; Woollings *et al*., 2018). These slow-moving, quasi-stationary and high amplitude Rossby waves can result in the persistence of weather conditions, including extreme heat waves and cold spells, such as those associated with blocking anticyclones (Vavrus *et al*., 2017; Brunner *et al*., 2018). Wang and Kuang (2019a, 2019b) have suggested a different mechanism that explains an increase in blocking as the jet stream migrates poleward in a warmer climate. They find that Rossby waves are compressed due to the shorter distance around the globe at higher latitudes, which makes them more likely to align and amplify, enhancing blocking.

Blocking anticyclones have a significant role in modulating the surface energy budget of the Greenland ice sheet (McLeod and Mote, 2015, 2016; Välisuo *et al*., 2018; Hofer *et al*., 2019). In addition to adiabatic warming from sinking air in the anticyclone (McLeod and Mote, 2015), diabatic contributions from increased cloud cover and moisture transport during the passage of the anticyclone provide energy for surface melting (Mattingly *et al*., 2018; Barrett *et al*., 2020). For example, anomalous blocking conditions over Greenland during July 2012 allowed for significant surface melting of the ice sheet (Figure 1) (Nghiem *et al*., 2012; Tedesco *et al*., 2013). As such, long-term warming over Greenland has resulted in increased melt (Tedesco *et al*., 2016), where the accelerated melt is closely linked to the increased advection of warm, moist airmasses (Fettweis *et al*., 2013; Hanna *et al*., 2014;

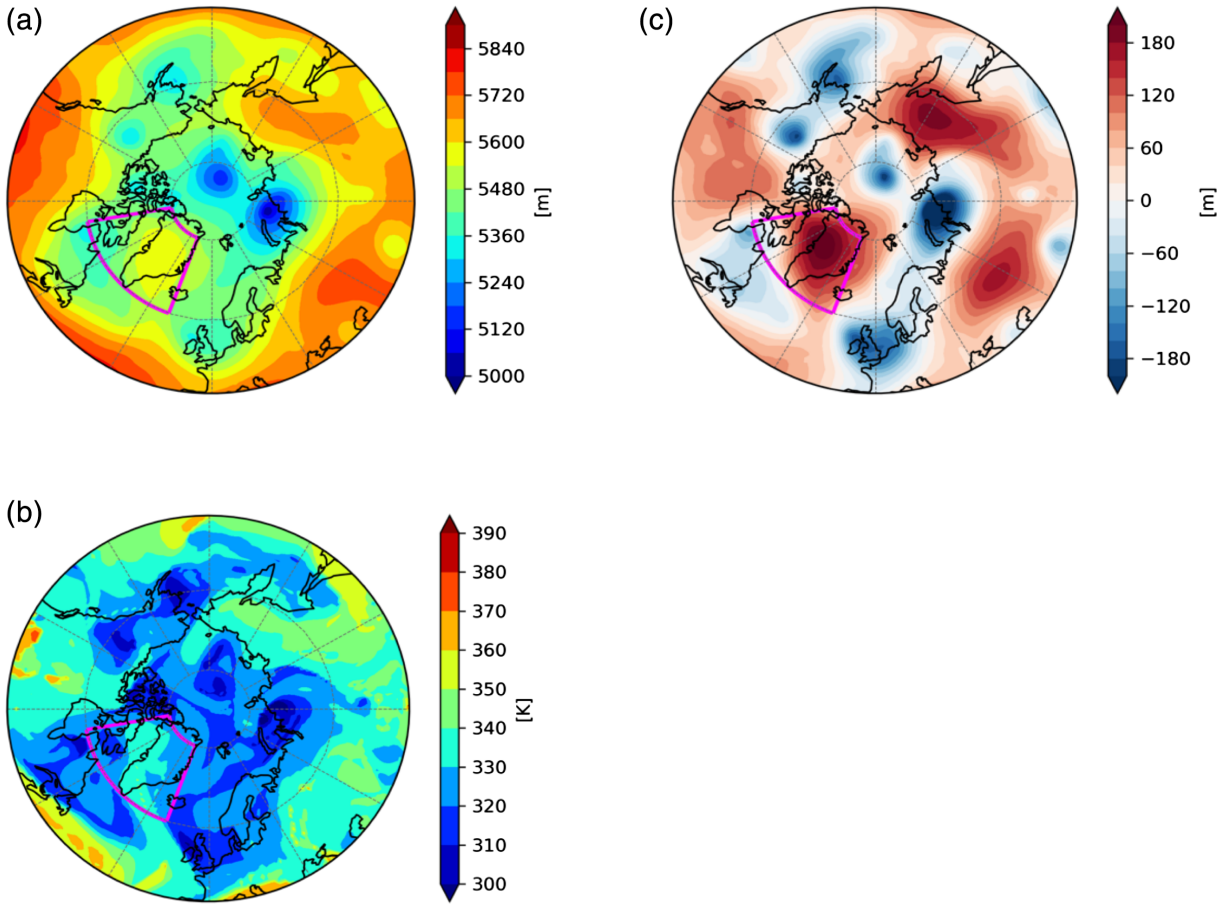

FIGURE 1 A Greenland blocking event on 11 July 2012 seen in (a) 500 hPa height, (b) 500 hPa height anomalies compared with the 1981–2010 JJA climatology, and (c) potential temperature at 2PVU. The box corresponds to the spatial extent of the GBI boundary

Mattingly *et al*., 2016; Delhasse *et al*., 2018; Hofer *et al*., 2019).

Since the mid-1990s, increased anticyclonic conditions have been observed over Greenland (Hanna *et al*., 2016; Tedesco *et al*., 2016; Hanna *et al*., 2018a, 2018b; Barrett *et al*., 2020). This trend has long been most notable in Northern Hemisphere summer (JJA) and winter (DJF) and corresponds to a decrease in the North Atlantic Oscillation (NAO) during this period (Hanna *et al*., 2015, 2018b). However, blocking is not generally well-represented throughout the Northern Hemisphere (Masato *et al*., 2013b; Davini and D'Andrea, 2016), where the historical increase in JJA blocking over Greenland, in particular, remains underestimated in most models from the fifth Coupled Model Intercomparison Project (CMIP5) (Hanna *et al*., 2018a). Furthermore, many global circulation models predict a decrease in JJA Greenland blocking (Hanna *et al*., 2018a), which may be caused by individual model representation of the NAO (Davini and Cagnazzo, 2014). Furthermore, cyclonic Rossby wave breaking, in particular, acts to promote a negative NAO and, thus, favourable conditions for Greenland blocking (Woollings *et al*., 2008; Strong and Magnusdottir, 2008; Masato *et al*., 2012; Davini and Cagnazzo, 2014; Hanna *et al*., 2018b). This becomes important as wave breaking events are becoming more frequent with a poleward shift in the jet stream (Jing and Banerjee, 2018), and where possible increases in cyclonic wave breaking appear to coincide with increases in blocking activity in the North Atlantic (Hanna *et al*., 2018b; Bowley *et al*., 2019).

Greenland blocking is commonly quantified using the Greenland blocking index (GBI) (e.g., Fang, 2004; Hanna *et al*., 2016, 2018a), which identifies 500 hPa height anomalies over Greenland (Figure 1a,b). Other commonly used metrics for quantifying blocking more generally across the globe include height-based indices such as those presented by Lejenäs and Økland (1983) and Tibaldi and Molteni (1990; hereafter TM90), likely popular due to their simple design and ability to identify instantaneous blocking conditions in a location. Another way to quantify blocking is to use a potential vorticity (PV)-potential temperature (Θ) method, such as that in Pelly and Hoskins (2003; hereafter PH03), which allows for a more dynamic approach to quantify blocking associated with Rossby wave breaking (Figure 1c) (Woollings *et al*., 2008; Masato *et al*., 2012, 2013a), due to the conservation and invertibility principles of PV (Hoskins *et al*., 1985). However, neither of the metrics described in TM90 and PH03 appear to have been used to look at Greenland blocking specifically, which has largely been examined using the GBI.

Geopotential height is sensitive to air temperature, as described by the hypsometric relationship (Petty, 2008). Furthermore, the local time rate of change in geopotential thickness is the sum of the individual contributions of temperature advection, adiabatic processes, and diabatic heating (Sutcliffe and Forsdyke, 1950; Lackmann, 2011). However, when considering the global mean, only the diabatic contribution remains relevant. It follows that the global mean trend in the 500 hPa height surface over recent decades should be largely reflective of the radiative forcing of the lower troposphere by elevated greenhouse gas concentrations. This leads to potential issues in discerning whether GBI-inferred changes in blocking over Greenland exist due to thermodynamic or dynamic processes. This has important implications for our current understanding of the relationship between atmospheric circulation and Greenland ice sheet surface mass balance, given that studies of long-term variability of Greenland blocking have largely been limited to analysis of the GBI.

Thus, to obtain an accurate picture of the role of atmospheric blocking in the recent acceleration of surface runoff from the Greenland ice sheet, it is essential to assess the robustness of observed trends in Greenland blocking through the lens of different metrics outside of the standard GBI definition, as each metric approaches blocking from a different dynamical perspective. We document our efforts to do so as follows: Section 2 provides a thorough description of each blocking metric used in this manuscript. Section 3 presents the main results of temporal changes in seasonal blocking frequency for each metric, as well as compares high and low blocking seasons across metrics. A brief discussion of the main findings, comparison to past studies, and a discussion of advantages of each metric used in this study is found in Section 4, with a summary of the findings in Section 5.

2 | METHODS

We analysed daily 1,200 UTC ECMWF Reanalysis version 5 (ERA5) data at a 1° spatial resolution for the period of January 1979 through December 2018 (Hersbach *et al*., 2020). These data have a vertical resolution of 137 model levels and are reported at 37 pressure levels. Variables used include: 500 hPa geopotential height (m), and temperature (K), potential vorticity ($Km^2 \cdot kg^{-1} \cdot s^{-1}$), u- and v-winds ($m \cdot s^{-1}$) at all pressure levels. Potential temperature was calculated at all pressure levels then linearly interpolated to a constant PV surface. The interpolation process starts at the top of the atmosphere, moves towards the surface, and stops searching after the first instance where the PV surface is found, as described in Bowley et al., (2019). Following

the algorithm described in Bowley et al., (2019), values of potential temperature greater than 460 K were set to missing and horizontal linear interpolation was used to fill in missing values in order to have spatially complete data required for identifying instantaneous blocking as described below. The surface used was 2 potential vorticity units (2PVU, 2×10^{-6} $Km^2 \cdot s^{-1} \cdot kg^{-1}$), which is representative of the dynamic tropopause in the mid- to high-latitudes (Hoskins *et al*., 1985; Morgan and Nielsen-Gammon, 1998).

2.1 | GBI

The GBI, defined as the mean 500 hPa geopotential height over a domain spanning 60–80°N and 20–80°W ($Z500_{GBI}$), is used as a measure of atmospheric blocking local to the Greenland ice sheet (Figure 1) (Hanna *et al*., 2013, 2014; McLeod and Mote, 2016). In this study, we examine seasonal trends in the GBI, as represented by ERA5, using standard meteorological seasons: September–November (SON), December–February (DJF), March–May (MAM), and June–August (JJA). To do so, we calculate the seasonal anomaly of the 500 hPa geopotential height field relative to the 1981–2010 reference period for each year at each grid point of the ERA5 record. We then take the area-weighted mean of those grid cells that fall within the GBI domain by weighting each observation by the cosine of its latitude to create a time series of the seasonal GBI anomaly, referred to hereafter as the raw GBI anomaly.

Because it is simply a measure of mean geopotential height, a positive trend in GBI does not necessarily equal an increase in blocking frequency. For example, anthropogenic forcing has caused an increase in globally averaged 500 hPa geopotential height (Christidis and Stott, 2015), suggesting a change in the background state of the atmosphere is likely at least partially responsible for recent upward GBI trends. To adjust for this changing background state and better isolate any dynamical contribution to the positive trend in the GBI since 1980 (Hanna *et al*., 2015, 2018a, 2018b), we subtract the globally averaged 500 hPa geopotential height ($Z500_G$), which includes the GBI domain, from the GBI for each season (similar to Christidis and Stott, 2015). This is performed by first calculating the seasonal, area-weighted, global-mean anomaly of the geopotential height field relative to 1981–2010, as outlined for the GBI above. We then subtract this seasonal global-mean anomaly from the corresponding seasonal GBI anomaly for each year. The resulting index, hereafter referred to as GBI-G, or the globally adjusted GBI, represents a measure of geopotential height over Greenland that has been adjusted to remove the influence of global geopotential height change:

$$GBI - G = Z500_{GBI} - Z500_G \quad (1)$$

Thus, any remaining trend in the residuals provides a better representation of changes in the GBI that are due to dynamic influences, such as a rise in the magnitude and frequency of Greenland blocking events, than does the raw GBI.

The approach outlined above represents one way to adjust the GBI for the influence of the radiative forcing of global warming on the background geopotential height field while still preserving any signal that would arise due to change in blocking frequency (i.e., dynamical contributions to $Z500_{GBI}$). Nevertheless, it likely still fails to fully capture the diabatic impact of global warming, as multiple radiative feedbacks operating at high latitudes cause an accelerated rate of warming relative to the rest of the globe, during Arctic amplification (Serreze and Barry, 2011; Pithan and Mauritsen, 2014). In other words, one would expect the zonally averaged increase in mid-to-lower tropospheric temperature, and thus the increase in the background 500 hPa geopotential height field, to be greater at high latitudes, such as those included in the GBI calculation, than the increase in global-mean geopotential height field. To account for this, we follow a similar process as that outlined above and previous work (see Hanna *et al*., 2018a) by subtracting the area-weighted mean geopotential height of the zonal band spanning the GBI domain (i.e., 60–80°N, $Z500_Z$) to create a second index, GBI-Z to account for changes in GBI with respect to the zonal band:

$$GBI - Z = Z500_{GBI} - Z500_Z \quad (2)$$

It is important to note that while use of this zonal band average better accounts for the impact of Arctic amplification on the background state, its limited area means that the trend in the GBI-Z is also reflective of the dynamic contributions of temperature advection and adiabatic processes. Consequently, use of this domain to adjust the GBI may result, to some degree, in the removal of the blocking signal that we seek to isolate.

2.2 | Tibaldi and Molteni index

The Tibaldi and Molteni index (TM) (referred to here as TM; see TM90) identifies in the 500 hPa field reversals of the geopotential height (Z) gradients to the north and south of a given latitude (ϕ) (Figure 1a). The southward gradient (GHGS) and northward gradient (GHGN) are calculated as

$$GHGS = \frac{Z(\phi_o) - Z(\phi_s)}{\phi_o - \phi_s} \quad (3a)$$

$$GHGN = \frac{Z(\phi_n) - Z(\phi_o)}{\phi_n - \phi_o} \quad (3b)$$

where $\phi_n = 80°N$ $\phi_o = 60°N$, $\phi_s = 40°N$. The calculations are repeated, by adding 4° (−4°) to each ϕ, to account for north (south) latitudinal variability in blocking. As described in TM90, for blocking conditions to be present at a given longitude, GHGS >0 and GHGN < −10 m/deg latitude for at least one of the calculations. We consider a day with blocking conditions for Greenland if the longitudinal extent of the block spans at least 12° longitude within the GBI domain, which is the minimal spatial extent required to be considered a block (TM90).

2.3 | Pelly and Hoskins index (PH)

Unlike GBI and TM90, which exclusively use geopotential height data, the Pelly and Hoskins Index (referred to here as Pelly and Hoskins index [PH]; see PH03) utilizes potential temperature (Θ) on a constant potential vorticity (PV) surface of 2 potential vorticity units (2PVU) to identify reversals of the meridional potential temperature gradient (Figure 1c). According to PH03, the blocking index, B, for a given longitude is calculated as

$$B = \frac{2}{\Delta\phi}\int_{\phi_o}^{\phi_o+\Delta\phi/2} \theta d\phi - \frac{2}{\Delta\phi}\int_{\phi_o-\Delta\phi/2}^{\phi_o} \theta d\phi \quad (4)$$

Where ϕ_o is the central blocking latitude and $\Delta\phi = 30°$ is the latitudinal range over which the gradient is calculated. Under this definition, $B > 0$ indicates a reversal of the gradient, thus corresponding to blocking. This method is argued to provide a more dynamic approach to identifying blocking events, as instantaneous blocking at a given longitude varies by latitude (PH03). Following PH03, ϕ_o is identified as the latitude of maximum climatological annual eddy kinetic energy (EKE) at 300 hPa (Figure 2). We apply a 2.5 to 10-day bandpass filter on the u- and v-winds prior to calculating annual EKE (Figure 2a). The 2.5 to 10-day filter best accounts for nonlinear synoptic baroclinic eddies (Blackmon and White, 1982), making it an appropriate range to calculate EKE and approximate the location of the eddy-driven jet. We calculate EKE as follows

$$EKE = \frac{1}{2}(u\prime + v\prime)^2 \quad (5)$$

where u' and v' are the bandpass filtered u- and v- winds. From here, we extract the maximum B value for $\phi_o = \phi_o +/- \Delta$, where $\Delta = 4°$, similar to the TM index, for each longitude. We refer to the use of this methodology as the original PH index for the rest of the article.

We note that based on Figure 2b, we repeated the same procedure using seasonal climatological mean EKE values to test whether the summer (JJA) blocking climatology is strongly influenced by seasonal changes in EKE, thus leading to an underestimation of blocking in JJA when compared with the annual mean EKE-based method as described in PH03. Hereafter, we refer to the seasonal EKE variation of the PH method as a modified

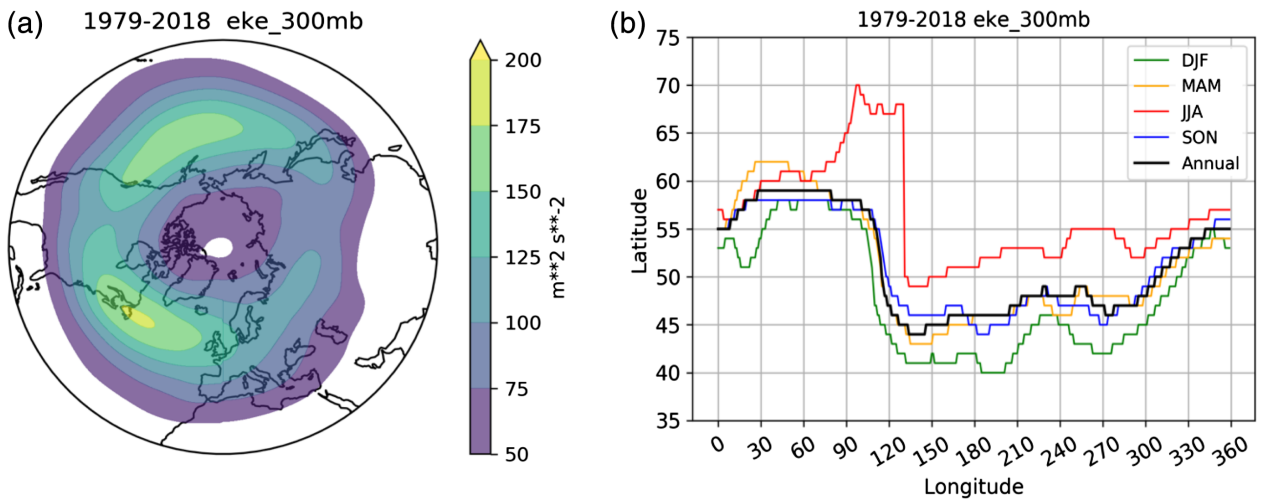

FIGURE 2 (a) Annual mean bandpass-filtered eddy kinetic energy (EKE) for 1979–2018. (b) Latitude of annual mean (black line) and seasonal mean EKE (coloured) at each longitude. Data were spatially smoothed with a Gaussian filter

(seasonal) PH index. For both variations on the PH index, we identify days in which 12° of longitude exhibits instantaneous blocking criteria within the GBI longitudinal domain. Although PH03 use a 15° longitudinal threshold, we opt to use 12° to maintain consistency between this methodology and that from TM90.

2.4 | Trend analysis

In an attempt to first recreate trends in GBI as established in past research (e.g., Hanna *et al*., 2015, 2018b; Barrett *et al*., 2020), to assess seasonal trends in GBI we use linear regression (Wilkinson and Rogers, 1973; Chambers, 1992). Given that both the TM90 and both PH03 methods are calculated daily and then concatenated into seasonal frequencies, we argue that using the non-parametric Mann-Kendall to compare these metrics with the GBI is necessary, so as to not assume the underlying independence and distributions of the data test (Mann, 1945; Kendall, 1975). An additional advantage to using the Mann-Kendall test over the linear regression is its ability to account for non-linear trends in environmental data. We propose that statistically significant trends in seasonal blocking shown from the Mann-Kendall test should act to further confirm existing linear trends in blocking shown from past research (e.g., Barnes *et al*., 2014; Hanna *et al*., 2015, 2018b).

We also note that the 1,200 UTC time step was selected to maintain consistency with previous daily blocking indices, particularly PH03. However, to assess whether the TM90 index is sensitive to the time step chosen, we applied a similar methodology as described below to a subset of years for 0000 UTC and find that no significant differences in seasonal trends were present (not shown). Although there are minor differences in seasonal totals in the TM90 at a daily level, given that the dynamic tropopause and 500 hPa levels used in this study are in the free atmosphere, we can assume diurnal effects are not present. We then choose to limit our analysis to only 1,200 UTC as day-to-day variability may be negligible in assessing seasonal trends.

3 | RESULTS

3.1 | Seasonal trends in GBI

As global temperatures increase, 500 hPa heights should also increase (Christidis and Stott, 2015). This is confirmed in Figure 3, where it is evident that both global and the 60–80°N zonal band of 500 hPa heights have increased since 1979 for all seasons. Moreover, the summary statistics of the linear regressions presented in Table 1 indicate that these positive trends are significant ($p < .05$) across all seasons for the global average, and for all seasons except spring for the zonal band, where $p = .076$. An increasing trend is likewise present in the raw GBI anomalies, which show more seasonal variability in 500 hPa height throughout the period (Figure 3). However, when considering the linear trend in raw GBI anomalies, only JJA exhibits a significant increase ($p < .05$) (Table 1). The positive trend in JJA is consistent with previous results (e.g., Hanna *et al*., 2018b). The remaining seasons all display a positive trend in GBI (Figure 3), but these trends are not significant at the 95% confidence level (Table 1).

We now examine the GBI after removing the global- and zonal-mean geopotential height signal to better isolate the dynamic response over Greenland from the large-scale thermodynamic forcing of global warming. For all seasons other than JJA, no significant trend was detected for either GBI-G or GBI-Z, suggesting no identifiable long-term trend in the GBI beyond that which is attributable to increasing temperature. However, it is worth noting that the GBI-Z exhibits a negative trend during SON with a *p*-value of .098, suggesting lower geopotential heights within the GBI domain relative to those at similar latitudes (Table 1). During JJA, there remains a positive trend in the GBI-G (Table 1); however, while still positive, the trend fails to meet the 95% confidence level when subtracting the zonal-mean geopotential height signal (Figure 4; Table 1). The positive GBI-G indicates that geopotential heights within the GBI domain have increased at a greater rate than would be expected due to the rise in global-mean temperature alone. This greater rate of change could be a sign of increased blocking activity, but it is also likely that it is at least partially attributable to amplified warming at high latitudes (Serreze and Francis, 2006). Hereafter, we will focus on the GBI-Z, as these may better capture dynamically driven changes in blocking over Greenland.

3.2 | Seasonal trends in other indices

Figure 5 shows the frequencies of the TM index and original and modified variations of the PH index. In all seasons, the TM index consistently underestimates days with blocking per season compared with both the PH-based indices. Both versions of the PH index likewise remain consistent in capturing blocking over Greenland for the transitional seasons (MAM and SON) but show differing frequencies of blocking in both DJF and JJA, with the greatest difference between the two PH indices in JJA. In particular, for DJF the original PH index results in higher

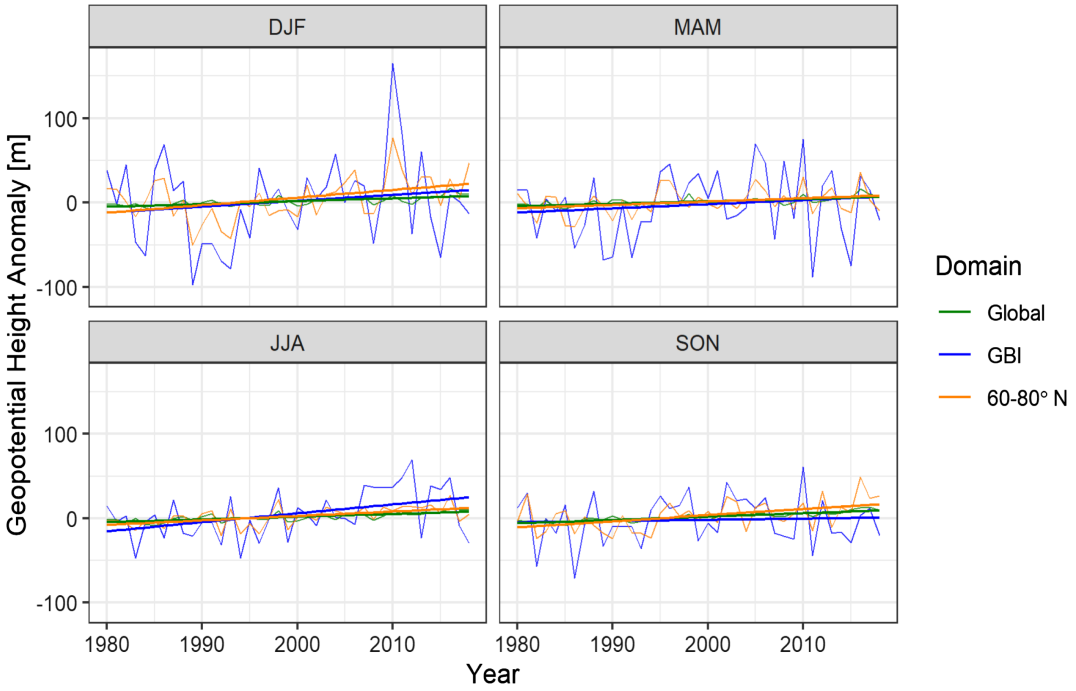

FIGURE 3 Raw seasonal GBI, global, 60–80°N zonal band of 500 hPa height anomalies. Time series and linear trend lines shown

blocking frequency when compared with the modified version of the index. In JJA, the modified index results in a higher seasonal blocking frequency when compared with the original PH metric.

Both PH metrics show increases in blocking frequency corresponding with the trends shown in the GBI during the period of 1990 onward for JJA (Figure 5). Notably, both the TM and PH indices indicate decreasing blocking in SON. Table 2 shows that based on a Mann-Kendall test to assess the presence of trends, negative trends exist during the SON season across all metrics, with a statistically significantly negative trend in the TM metric ($p < .05$). The raw GBI anomaly, however, indicates increasing blocking conditions in all seasons, except SON, with these trends being significant in JJA (Figure 5). Furthermore, for JJA, the original PH index suggests a decrease in blocking, whereas the modified PH index is more consistent with other indices by suggesting a positive trend. Across the different metrics, with the exception of the raw GBI anomalies, negative trends in blocking frequency, although not statistically significant, are present for both DJF and SON (Figure 5 and Table 2).

We show in Figure 6 that the different blocking metrics are relatively consistent in identifying abnormally high or low blocking seasons, particularly in DJF and MAM. As also shown in Figure 5, discrepancies exist between the TM- and PH-based indices for JJA and SON regarding blocking frequency, suggesting either the TM index may underestimate, or the PH-based indices overestimate total blocking frequency over Greenland in JJA and SON. For SON, the TM index shows anomalously low blocking frequencies compared with both the GBI and PH indices during the period of 1990–2005. It is possible that this underestimation of blocking by the TM index during this period may be contributing to the statistically significant decreasing trend in SON blocking when using the TM metric, and we believe this warrants further investigation. Finally, there are inconsistencies between the different metrics during JJA during 2007–2012. In particular, the GBI is consistently higher during this period, but the cause of this remains unclear.

Differences between TM-based blocking compared with the PH-based metrics and GBI are also present in JJA (Figure 6) and are particularly noteworthy in the context of individual events. In July 2012, for instance, the Greenland ice sheet experienced record surface melting (Nghiem *et al.*, 2012), where much of this melting was aided by consistently strong anticyclone activity over the region (Tedesco *et al.*, 2013). Blocking anomalies in JJA 2012 exceeded 2.5 standard deviations above average, according to the raw GBI, GBI-Z, and both PH indices (Figure 6). We also note the apparent underestimation of PH-based blocking compared with the GBI and TM indices during the period of 1995 to 2003 (Figure 6). This period of time further illustrates, much like the period of 1990 to 2005 for SON, that no single blocking metric may fully capture Greenland blocking.

		GBI	Global	GBI-G	Zonal	GBI-Z
DJF	*p*	.338	**.000**	.612	**.010**	.703
	r	0.158	0.707	0.084	0.406	−0.063
	r^2	0.025	0.499	0.007	0.165	0.004
	m	0.705	0.338	0.367	0.904	−0.199
	y_0	−1,406.830	−674.021	−732.800	−1801.350	394.500
MAM	*p*	.402	**.000**	.726	.076	.826
	r	0.138	0.641	0.058	0.288	0.036
	r^2	0.019	0.411	0.003	0.083	0.001
	m	0.493	0.290	0.203	0.395	0.098
	y_0	−988.034	−579.350	−408.700	−788.563	−199.500
JJA	*p*	**.006**	**0.000**	**.049**	**.000**	.073
	r	0.431	0.734	0.318	0.543	0.291
	r^2	0.185	0.538	0.101	0.295	0.085
	m	1.063	0.321	0.741	0.528	0.534
	y_0	−2,118.970	−640.398	−1,479.000	−1,053.660	−1,065.000
SON	*p*	.725	**.000**	.511	**.003**	.098
	r	0.058	0.856	−0.109	0.467	−0.269
	r^2	0.003	0.733	0.012	0.218	0.072
	m	0.143	0.402	−0.259	0.722	−0.578
	y_0	−288.568	−801.942	513.400	−1,439.420	1,151.000

TABLE 1 Statistics associated with the linear least squares regression analysis for the raw seasonal GBI calculation (GBI), global mean (global) and 60 to 80°N zonal mean (zonal) 500 hPa heights and the adjusted seasonal GBI anomalies using the global mean height (GBI-G) and the 60°N to 80°N zonal band height change (GBI-Z)

Note: Included in the table are the *p* values (*p*), r values (r), r-squared (r^2), slope of the trend (m), and y-intercept (y_0). Trends are considered significant for $p < .05$ and are indicated by bolded values.

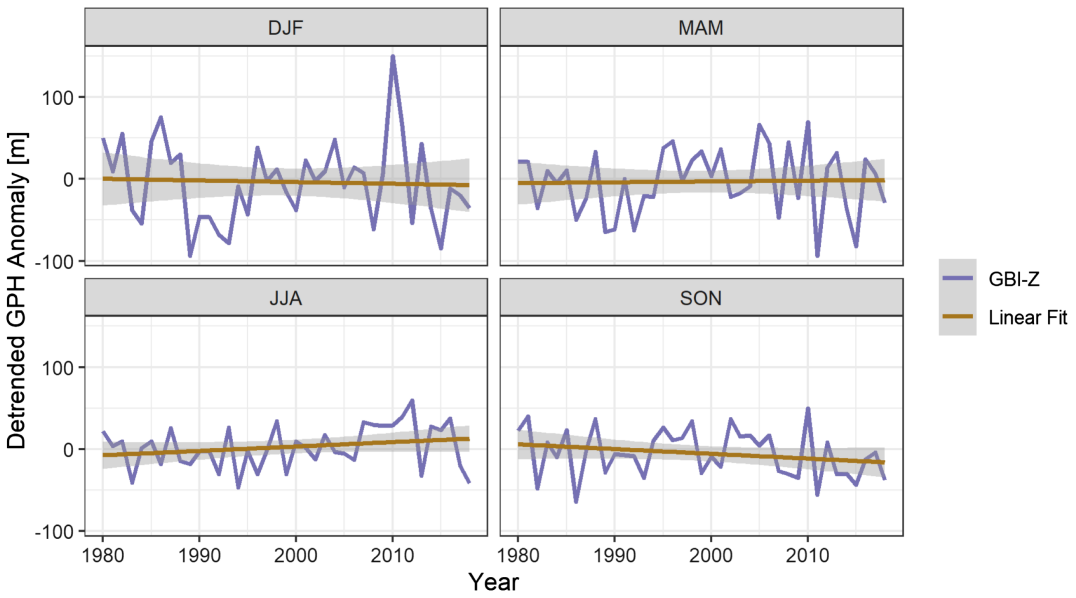

FIGURE 4 Seasonal mean GBI-Z and linear trend. The grey shading indicates the 95% confidence interval of the linear trend

Finally, we apply a 5-year running mean to the seasonal blocking frequency anomalies, similar to that of Hanna *et al.* (2018a), and those are shown in Figure 7. The different metrics are consistent in showing the temporal pattern of trends for DJF and MAM (Figure 7); however, only the raw GBI anomalies for DJF are

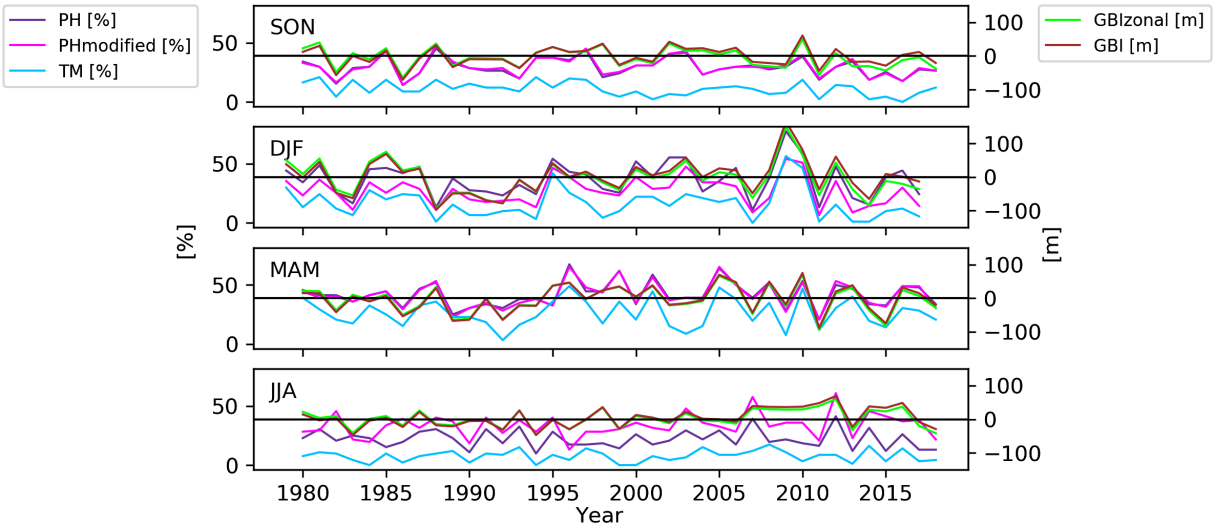

FIGURE 5 Time series of seasonal frequency of blocking (%) for the TM, traditional PH, and modified PH indices calculated as the total number of days per season with blocking criteria met (on the left y-axis). The monthly GBI anomalies (in meters) for the raw GBI and GBI-Z are associated with the rightmost y-axis. Note: The horizontal line corresponds to where y = 0 [m] for the GBI anomaly calculations, associated with the rightmost y-axis

increasing significantly ($p = .0054$**)** (Table 3). A negative trend is also shown in SON (Figure 7), and this trend is significant for the TM index ($p = .0001$) (Table 3). During the period of 2000 to 2007, the TM index shows less blocking compared with the PH and GBI metrics, with standardized blocking anomalies of ~1.5 standard deviations below normal. Most notably, the significant increase in blocking is present in JJA for all metrics, except the original PH index (Table 3). It appears that the GBI-based metrics (including raw and both adjusted methods) show a stronger increase in blocking since the mid-1990s, which is consistent with findings from Hanna *et al.* (2018a) and Barrett *et al.* (2020). Furthermore, the GBI-based metrics from 2010 onward diverge from the other indices, with a peak in standardized blocking frequency (greater than 1.5 *SD*) occurring in 2012; discerning the cause of this divergence warrants future investigation.

4 | DISCUSSION

To help explain differences in blocking frequencies in some seasons instead of others, it is necessary to consider how different metrics capture certain types of blocking. For example, PH03 note a distinct underestimation of Omega blocking patterns identified in the Pacific using the methodology of TM90 compared with their PV- Θ approach to blocking identification. In their discussion, PH03 attribute differences in climatology to storm tracks commonly occurring further south of the blocking latitude used in TM90. We note that in the North Atlantic region, seasonal variation of EKE appears to exhibit some influence on the skill of the PV- Θ indexing method in identifying individual, including significant, blocking events, which are not captured when considering annual mean EKE (as done in PH03), and when using a constant latitude of 60°N (as in TM90).

We also test the robustness of the observed positive trend in summertime Greenland blocking using the different metrics. We find that the metrics used in this study show a positive trend in JJA blocking observed in previous studies, with statistically significant positive trends only exhibited for the raw GBI. Observed increases in temperatures over the GBI domain have resulted in an increase in geopotential heights in accordance with the hypsometric relationship (e.g., Tedesco *et al.*, 2016), and corresponds to increases in extreme JJA and DJF blocking shown in Barrett et al., (2020). In particular, our results appear to support this by indicating increases in GBI during summer, which is consistent with findings from Hanna *et al.* (2016), Hanna *et al.*, 2018a). Likewise, the lack of robust trends in seasonal blocking frequency when considering other metrics for Greenland, specifically, is generally consistent with previous findings (e.g., Barnes, 2013; Barnes *et al.*, 2014), suggesting there is no clear observed linear trend in Northern Hemisphere blocking. After applying a 5-year running mean, the original PH index does not capture the increase in JJA blocking to the extent that the adjusted PH index does and, as described above, may partially be a factor of changes in storm tracks and EKE. Furthermore, how the individual metrics each define blocking may impact their

TABLE 2 Results from an original Mann-Kendall test for presence of trends, using standardized seasonal blocking frequency anomalies

		GBI	GBI-Z	PH	PH_modified	TM
SON	*p*	.8846	.0999	.3504	.4375	**.0230**
	z	−0.1452	−1.6452	−0.9338	−0.7764	−2.2734
	Tau	−0.0175	−0.1849	−0.1053	−0.0877	−0.2537
	s	−13	−137	−78	−65	−188
	var_s	6,833.7	6,833.7	6,800.0	6,795.0	6,766.0
	m	−0.0900	−0.8116	−0.0952	−0.0833	−0.1935
DJF	*p*	.5136	.5453	.9614	.7991	.1671
	z	0.6532	−0.6048	−0.0484	−0.2546	−1.3815
	tau	0.0742	−0.0688	−0.0067	−0.0297	−0.1552
	s	55	−51	−5	−22	−115
	var_s	6,833.7	6,833.7	6,823.7	6,804.7	6,809.0000
	m	0.4213	−0.4825	0.0000	0.0000	−0.1786
MAM	*p*	.3838	.7348	.5853	.5940	.7253
	z	0.8710	0.3387	0.5456	0.5330	−0.3514
	tau	0.0985	0.0391	0.0621	0.0607	−0.0405
	s	73	29	46	45	−30
	var_s	6,833.7	6,833.7	6,802.7	6,814.3	6,810.0000
	m	0.5861	0.1912	0.0769	0.1071	−0.0500
JJA	*p*	**.0119**	.1755	.2700	.2252	.8078
	z	2.5161	1.3548	−1.1031	1.2129	0.2433
	tau	0.2821	0.1525	−0.1242	0.1363	0.0283
	s	209	113	−92	101	21
	var_s	6,833.7	6,833.7	6,806.0	6,797.7	6,759.0000
	m	1.0656	0.5374	−0.1111	0.1429	0.0000

Note: Result statistics include the *p*-value (*p*), normalized test statistic (z), Kendall tau (tau), the Mann-Kendall score (s), the variance of the MK score (var_s), and Sen's slope (m). Trends are considered statistically significant for $p < .05$ and are indicated in bolded text.

representation of the temporal variability in Greenland blocking. Our results suggest a minor seasonal decrease in GBI during SON, consistent with findings from Hanna *et al*. (2016). Likewise, similar trends are seen in other blocking metrics.

Although there exists seasonal asymmetry in blocking trends when using the 5-year running mean, with significant increases in blocking occurring in JJA compared with other seasons, we posit that these changes in frequency may be manifestations of previously suggested hypotheses summarized in Coumou *et al*. (2018), particularly the decline in EKE (Coumou *et al*., 2015; Hoskins and Woollings, 2015) and by the latitudinal shifting of jet streams (e.g., Barnes and Polvani, 2013, 2015; Kennedy *et al*., 2016; Iqbal *et al*., 2018), including shifts in position from wave breaking (e.g., Barnes *et al*., 2010; Ronalds *et al*., 2018). North Atlantic blocking, in particular appears most sensitive to shifts in the jet during the summer season (Barnes and Polvani, 2015; Kennedy *et al*., 2016). Given the prominent decrease in EKE during summer (e.g., Coumou *et al*., 2015), dynamic drivers such as increases in wave breaking activity may drive changes in blocking more in summer than in winter (e.g., Hanna *et al*., 2016, 2018b; Bowley *et al*., 2019), thus leading to the increase in summer blocking over Greenland. While we do not attempt to attribute observed changes in blocking to one particular hypothesis, we do acknowledge that future work should look to discern how changes in atmospheric circulation in the North Atlantic are driven by various mechanisms either by examining current hypotheses separately or in combination with each other.

The subset of blocking metrics analysed in this study does not include all available options for describing the frequency of blocking. However, we do show inconsistencies in blocking frequency across different metrics, which is important given the implications of blocking on the surface mass balance of Greenland with climate change. In summary, inconsistencies in how Greenland

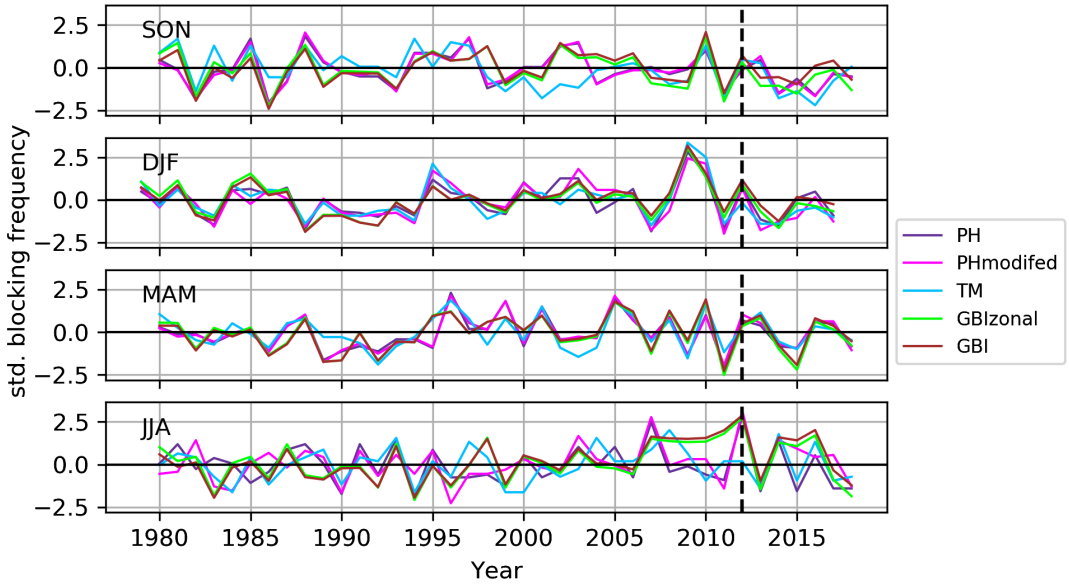

FIGURE 6 Standardized seasonal blocking frequency, with respect to the 1981–2010 (1980–2009 for DJF) reference period. Year refers to the year in which December occurred. The year 2012 is highlighted with a dashed black line

FIGURE 7 Time series of 5-year running mean of standardized seasonal blocking frequency anomalies. Year refers to the year in which December occurred. The year of 2012 is highlighted with the dashed black line

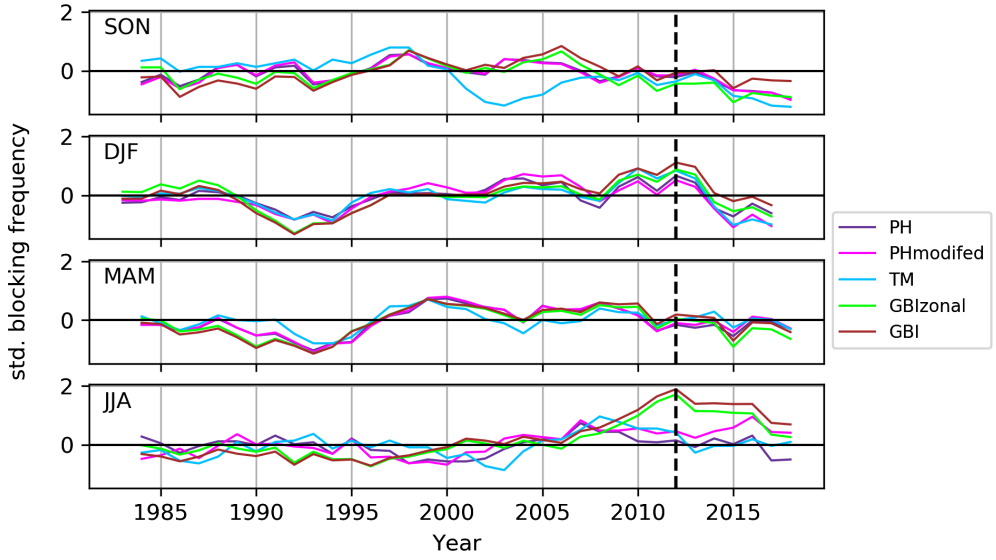

blocking is represented by various blocking metrics demonstrate the need to carefully consider which metric may be most useful for a particular research design. We highlight some key advantages and disadvantages below, acknowledging that many of these remain specific to the aforementioned results.

The GBI presents an anomaly-type of approach to blocking through the use of mean 500 hPa geopotential height over a region. This is advantageous due to its simplicity in the calculation in representing mean conditions of the atmosphere, allowing it to be calculated at timescales of seasonal to sub-daily. However, this method could be influenced by long-term changes in temperature, which could yield an overestimation of blocking activity (due to higher heights) over Greenland. Accounting for long term changes in air temperature and consequently, geopotential height, may aid in more realistic estimates of blocking activity over Greenland.

The TM methodology to identify blocking works well with sub-daily to daily scales by simply calculating the difference in meridional 500 hPa geopotential height about a constant latitude. This type of method also allows for instantaneous blocking conditions to be identified at a given longitude for a given time step, making it more

TABLE 3 Same as Table 2, but for using the 5-year running mean of seasonal standardized anomalies

		GBI	GBI-Z	PH	PH_modified	TM
SON	*p*	.1475	.0736	.1216	.2272	**.0001**
	z	1.4485	−1.7894	−1.5481	−1.2075	−3.9358
	tau	0.1731	−0.2134	−0.1849	−0.1445	−0.4672
	s	103	−127	−110	−86	−278
	var_s	4,958.3	4,958.3	4,957.3	4,955.3	4,953.3
	m	0.0099	−0.0154	−0.0109	−0.0108	−0.0348
DJF	*p*	**.0054**	.4954	.1640	2112	.4774
	z	2.7835	0.6817	1.3917	1.2502	0.7105
	tau	0.3311	0.0824	0.1664	0.1496	0.0857
	s	197	49	99	89	51
	var_s	4,958.3	4,958.3	4,958.3	4,954.3	4,951.6667
	m	0.0247	0.0076	0.0136	0.0141	0.0064
MAM	*p*	.0995	.5136	.3063	.2441	.5135
	z	1.6474	0.6533	1.0229	1.1648	0.6534
	tau	0.1966	0.0790	0.1227	0.1395	0.0790
	s	117	47	73	83	47
	var_s	4,958.3	4,958.3	4,954.3	4,956.3	4,956.3333
	m	0.0170	0.0070	0.0077	0.0094	0.0033
JJA	*p*	**.0000**	**.0000**	.7545	**.0000**	**.0097**
	z	5.5386	4.3172	0.3127	4.1330	2.5864
	tau	0.6571	0.5126	0.0387	0.4908	0.3076
	s	391	305	23	292	183
	var_s	4,958.3	4,958.3	4,950.3	4,957.3	4,951.6667
	m	0.0589	0.0402	0.0019	0.0268	0.0140

Note: Trends are considered statistically significant for $p < .05$ and are indicated in bolded text.

advantageous for spatiotemporal analysis of blocking. The use of a constant latitude, such as 60°N as used in this study and TM90, means that underestimation of blocking activity is likely in regions where strong shifts in the jet stream occur on seasonal or interannual timescales.

The PH03 method utilizes the latitudinal variability in annual storm tracks to serve as a proxy of blocking location. Thus, the index is calculated as the average meridional difference about a latitude of potential temperature on a constant potential vorticity surface at a given longitude, providing instantaneous blocking conditions at a given longitude at daily or sub-daily levels. Likewise, it is suggested that PV-Θ approach allows for representing the conservation and invertibility of PV, thus allowing a constant PV surface better identify features which act to maintain the block. There are two main disadvantages of the PH03 blocking method. First, data sets with potential temperatures interpolated to a constant PV surface may not readily available. Second, the use of annual average EKE limits blocking accuracy in areas where there are strong seasonal shifts in the jet stream. As shown in this study, the use of seasonal mean EKE values may better capture specific, anomalous events over Greenland where the eddy-driven jet is shifted outside of its annual climatology.

5 | CONCLUSION

Blocking anticyclones play an important role in distributing heat and moisture in the mid- to high-latitudes, and they have a large impact on the Greenland ice sheet in terms of regulating mass balance. Various metrics have been designed to capture atmospheric flow blocking, where some focus on geopotential height data while others use a PV-based framework for identifying events. Greenland blocking, specifically, has largely been examined using only the GBI. In this study, we identify seasons of high and low blocking over the GBI domain using three commonly used blocking metrics (the GBI, the TM index, and the PH index). We further compare

these three metrics to test the robustness of the observed positive trends in GBI frequency.

In general, most metrics confirm no significant trend in seasonal blocking, with the exception of the GBI, which is broadly consistent with previous findings. The GBI-Z, the Tibaldi and Molteni (1990)-based blocking index, and the Pelly and Hoskins (2003)-based blocking indices using both annual and seasonal variations of EKE-based blocking latitude do not reveal the positive trend that shows up in the GBI. Instead, all suggest possible decreases in blocking frequency in colder seasons (SON and DJF) and increases in MAM and JJA. These trends are not considered statistically significant for all seasons (except SON for TM). On the other hand, we find a statistically significant positive trend in JJA blocking over Greenland, with possible increasing blocking frequency also present in DJF and MAM when seasonal frequencies are temporally-smoothed using a 5-year running mean. This significant positive trend is prevalent for all metrics except for PH03. These finding are likewise consistent with previous findings focused on trends in GBI.

When considering how these metrics compare with each other, it appears that the TM index may underestimate blocking trends of increased summer blocking compared with the GBI and PH-based approaches. Moreover, interannual variability exists within each metric, which appears to not remain consistent across metrics, leading us to question drivers of blocking in years of inconsistent blocking representation. It is possible the variability of storm tracks at both the seasonal and interannual level may shift the jet stream north or south and lead to over- or under-estimation of blocking when using metrics based on a constant blocking latitude. This becomes important when trying to identify individual historical events of interest, such as blocking on July 10–11, 2012. However, changes in synoptic scale EKE near Greenland have not been fully considered in this study and is an area which warrants further investigation.

Overall, we demonstrate relative consistency of different blocking metrics in representing recent trends in blocking over Greenland. We encourage an ensemble-type approach to consider the various limitations which may be present in using a single metric. In particular, we demonstrate a weakness in using the raw GBI values to assess trends, as there is evidence of increasing trends in 500 hPa height both globally and for the zonal band associated with the GBI domain. Inconsistent significant seasonal trends become present when using the zonally adjusted GBI and other metrics, which do not align with the trends seen in the raw GBI values. Likewise, this increase in blocking is not present across all seasons (i.e., SON) when using the other metrics, which contrasts with the hypothesis that increased warming should lead to more blocking. Consequently, increases in the raw GBI more generally may be manifestations of global increases in temperatures instead of changes in synoptic conditions defined to be a Greenland block. These results then imply a lack of observational evidence in supporting the hypothesis of increases in blocking, particularly Greenland blocking, due to Arctic amplification. Because the ability to represent blocking over Greenland presents issues with understanding mass balance estimates of the ice sheet due to climate change as represented in climate models, the results presented in this paper should benefit those wishing to consider relationships between atmospheric circulation patterns and mass balance of Greenland in both historical and future context.

ACKNOWLEDGEMENTS

This work was supported by Strategic Environmental Research and Development Program project number RC18-1658 and NSF Arctic Systems Science award number 1900324. The authors declare no conflict of interest. The authors thank three anonymous reviewers whose insightful comments greatly improved this article.

ORCID

Lori J. Wachowicz https://orcid.org/0000-0001-5483-0462

Jonathon R. Preece https://orcid.org/0000-0002-4463-7770

Bradford S. Barrett https://orcid.org/0000-0002-5575-9052

REFERENCES

Barnes, E.A., Hartmann, D.L., Frierson, D.M. and Kidston, J. (2010) Effect of latitude on the persistence of eddy-driven jets. *Geophysical Research Letters*, 37(11), L11804. https://doi.org/10.1029/2010GL043199.

Barnes, E.A. and Polvani, L. (2013) Response of the midlatitude jets, and of their variability, to increased greenhouse gases in the CMIP5 models. *Journal of Climate*, 26(18), 7117–7135. https://doi.org/10.1175/jcli-d-12-00536.1.

Barnes, E.A. (2013) Revisiting the evidence linking Arctic amplification to extreme weather in midlatitudes. *Geophysical Research Letters*, 40(17), 4734–4739. https://doi.org/10.1002/grl.50880.

Barnes, E.A., Dunn-Sigouin, E., Masato, G. and Woollings, T. (2014) Exploring recent trends in northern hemisphere blocking. *Geophysical Research Letters*, 41(2), 638–644. https://doi.org/10.1002/2013GL058745.

Barnes, E.A. and Polvani, L.M. (2015) CMIP5 projections of Arctic amplification, of the north American/North Atlantic circulation, and of their relationship. *Journal of Climate*, 28(13), 5254–5271. https://doi.org/10.1175/JCLI-D-14-00589.1.

Barrett, B.S., Henderson, G.R., McDonnell, E., Henry, M. and Mote, T.L. (2020) Extreme Greenland blocking and

high-latitude moisture transport. *Atmospheric Research Letters*, 21, e1002. https://doi.org/10.1002/asl.1002.

Blackmon, M.L. and White, G.H. (1982) Zonal wavenumber characteristics of northern hemisphere transient eddies. *Journal of the Atmospheric Sciences*, 39, 1985–1998. https://doi.org/10.1175/1520-0469(1982)039<1985:ZWCONH>2.0.CO;2.

Bowley, K.A., Gyakum, J.R. and Atallah, E.H. (2019) A new perspective toward cataloging northern hemisphere Rossby wave breaking on the dynamic Tropopause. *Monthly Weather Review*, 147, 409–431. https://doi.org/10.1175/MWR-D-18-0131.1.

Brunner, L., Schaller, N., Anstey, J., Sillmann, J. and Steiner, A.K. (2018) Dependence of present and future European temperature extremes on the location of atmospheric blocking. *Geophysical Research Letters*, 45, 6311–6320. https://doi.org/10.1029/2018GL077837.

Chambers JM, 1992. Linear models. Chapter 4 of Statistical Models in S eds J. M. Chambers and T. J. Hastie, Wadsworth & Brooks/Cole.

Christidis, N. and Stott, P.A. (2015) Changes in the geopotential height at 500 hPa under the influence of external climatic forcings. *Geophysical Research Letters*, 42, 10–10,806. https://doi.org/10.1002/2015GL066669.

Coumou, D., Lehmann, J. and Beckmann, J. (2015) The weakening summer circulation in the northern hemisphere mid-latitudes. *Science*, 348(6232), 324–327. https://doi.org/10.1126/science.1261768.

Coumou, D., Di Capua, G., Vavrus, S., Wang, L. and Wang, S. (2018) The influence of Arctic amplification on mid-latitude summer circulation. *Nature Communications*, 9(1), 1–12. https://doi.org/10.1038/s41467-018-05256-8.

Dai, A., Luo, D., Song, M. and Liu, J. (2019) Arctic amplification is caused by sea-ice loss under increasing CO2. *Nature Communications*, 10(1), 121. https://doi.org/10.1038/s41467-018-07954-9.

Davini, P. and Cagnazzo, C. (2014) On the misinterpretation of the North Atlantic oscillation in CMIP5 models. *Climate Dynamics*, 43, 1497–1511. https://doi.org/10.1007/s00382-013-1970-y.

Davini, P. and D'Andrea, F. (2016) Northern hemisphere atmospheric blocking representation in global climate models. *Journal of Climate*, 29, 8823–8840. https://doi.org/10.1175/JCLI-D-16-0242.1.

Delhasse, A., Fettweis, X., Kittel, C., Amory, C. and Agosta, C. (2018) Brief communication: impact of the recent atmospheric circulation change in summer on the future surface mass balance of the Greenland ice sheet. *The Cryosphere*, 12, 3409–3418. https://doi.org/10.5194/tc-2018-65.

Fang ZF. 2004. Statistical relationship between the northern hemisphere sea ice and atmospheric circulation during wintertime. In Observation, Theory and Modeling of Atmospheric Variability: Selected Papers of Nanjing Institute of Meteorology Alumni in Commemoration of Professor Jijia Zhang (pp. 131–141).

Fettweis, X., Hanna, E., Lang, C., Belleflamme, A., Erpicum, M. and Gallée, H. (2013) Brief communication: important role of the midtropospheric atmospheric circulation in the recent surface melt increase over the Greenland ice sheet. *The Cryosphere*, 7, 241–248. https://doi.org/10.5194/tc-7-241-2013.

Francis, J.A. and Vavrus, S.J. (2012) Evidence linking Arctic amplification to extreme weather in mid-latitudes. *Geophysical Research Letters*, 39, n/a. https://doi.org/10.1029/2012GL051000.

Francis, J.A. and Vavrus, S.J. (2015) Evidence for a wavier jet stream in response to rapid Arctic warming. *Environmental Research Letters*, 10, 14005. https://doi.org/10.1088/1748-9326/10/1/014005.

Hanna, E., JM Jones, J.C., Mernild, S.H., LWood, K. and Steffen, P. H. (2013) The influence of North Atlantic atmospheric and oceanic forcing effects on 1900-2010 Greenland summer climate and ice melt/runoff. *International Journal of Climatology*, 33(4), 862–880. https://doi.org/10.1002/joc.3475.

Hanna, E., Fettweis, X., Mernild, S.H., Cappelen, J., Ribergaard, M. H., Shuman, C.A., Steffen, K., Wood, L. and Mote, T.L. (2014) Atmospheric and oceanic climate forcing of the exceptional Greenland ice sheet surface melt in summer 2012. *International Journal of Climatology*, 34, 1022–1037. https://doi.org/10.1002/joc.3743.

Hanna, E., Cropper, T.E., Jones, P.D., Scaife, A.A. and Allan, R. (2015) Recent seasonal asymmetric changes in the NAO (a marked summer decline and increased winter variability) and associated changes in the AO and Greenland blocking index. *International Journal of Climatology*, 35, 2540–2554. https://doi.org/10.1002/joc.4157.

Hanna, E., Cropper, T.E., Hall, R.J. and Cappelen, J. (2016) Greenland blocking index 1851–2015: a regional climate change signal. *International Journal of Climatology*, 36, 4847–4861. https://doi.org/10.1002/joc.4673.

Hanna, E., Fettweis, X. and Hall, R.J. (2018a) Brief communication: recent changes in summer Greenland blocking captured by none of the CMIP5 models. *The Cryosphere*, 12, 3287–3292. https://doi.org/10.5194/tc-12-3287-2018.

Hanna, E., Hall, R.J., Cropper, T.E., Ballinger, T.J., Wake, L., Mote, T. and Cappelen, J. (2018b) Greenland blocking index daily series 1851–2015: analysis of changes in extremes and links with North Atlantic and UKclimate variability and change. *International Journal of Climatology*, 38, 3546–3564. https://doi.org/10.1002/joc.5516.

Hersbach, H., Bell, B., Berrisford, P., Hirahara, S., Horányi, A., Muñoz-Sabater, J., Nicolas, J., Peubey, C., Radu, R., Schepers, D., Simmons, A., Soci, C., Abdalla, S., Abellan, X., Balsamo, G., Bechtold, P., Biavati, G., Bidlot, J., Bonavita, M., Chiara, G., Dahlgren, P., Dee, D., Diamantakis, M., Dragani, R., Flemming, J., Forbes, R., Fuentes, M., Geer, A., Haimberger, L., Healy, S., Hogan, R.J., Hólm, E., Janisková, M., Keeley, S., Laloyaux, P., Lopez, P., Lupu, C., Radnoti, G., Rosnay, P., Rozum, I., Vamborg, F., Villaume, S. and Thépaut, J.N. (2020) The ERA5 global reanalysis. *Quarterly Journal of the Royal Meteorological Society*, 146, 1999–2049. https://doi.org/10.1002/qj.3803.

Hofer, S., Tedstone, A.J., Fettweis, X. and Bamber, J.L. (2019) Cloud microphysics and circulation anomalies control differences in future Greenland melt. *Nature Climate Change*, 9, 523–528. https://doi.org/10.1038/s41558-019-0507-8.

Hoskins, B.J., McIntyre, M.E. and Robertson, A.W. (1985) On the use and significance of isentropic potential vorticity maps. *Quarterly Journal of the Royal Meteorological Society*, 111, 877–946.

Hoskins, B. and Woollings, T. (2015) Persistent extratropical regimes and climate extremes. *Current Climate Change Reports*, 1(3), 115–124. https://doi.org/10.1007/s40641-015-0020-8.

Iqbal, W., Leung, W.N. and Hannachi, A. (2018) Analysis of the variability of the North Atlantic eddy-driven jet stream in

CMIP5. *Climate Dynamics*, 51(1–2), 235–247. https://doi.org/10.1007/s00382-017-3917-1.

Jing, P. and Banerjee, S. (2018) Rossby wave breaking and isentropic stratosphere-troposphere exchange during 1981–2015 in the northern hemisphere. *Journal of Geophysical Research-Atmospheres*, 123 (17), 9011–9025. https://doi.org/10.1029/2018JD028997.

Kendall, M. (1975) Rank correlation measures. *Charles Griffin, London*, 202, 15.

Kennedy, D., Parker, T., Woollings, T., Harvey, B. and Shaffrey, L. (2016) The response of high impact blocking weather systems to climate change. *Geophysical Research Letters*, 43, 7250–7258. https://doi.org/10.1002/2016GL069725.

Lackmann, G. (2011) *Midlatitude Synoptic Meteorology*. Boston MA: American Meteorological Society.

Lejenäs, H. and Øakland, H. (1983) Characteristics of northern hemisphere blocking as determined from long time series of observational data. *Tellus*, 35, 350–362. https://doi.org/10.1111/j.1600-0870.1983.tb00210.x.

Luo, D., Chen, X., Dai, A. and Simmonds, I. (2018) Changes in atmospheric blocking circulations linked with winter Arctic warming: a new perspective. *Journal of Climate*, 31, 7661–7678. https://doi.org/10.1175/JCLI-D-18-0040.1.

Mann, H.B. (1945) Nonparametric tests against trend. *Econometrica: Journal of the Econometric Society*, 13, 245–259. https://doi.org/10.2307/1907187.

Masato, G., Hoskins, B.J. and Woollings, T.J. (2012) Wave-breaking characteristics of midlatitude blocking. *Quarterly Journal of the Royal Meteorological Society*, 138, 1285–1296. https://doi.org/10.1002/qj.990.

Masato, G., Hoskins, B.J. and Woollings, T. (2013a) Wave-breaking characteristics of northern hemisphere winter blocking: a two-dimensional approach. *Journal of Climate*, 26, 4535–4549. https://doi.org/10.1175/JCLI-D-12-00240.1.

Masato, G., Hoskins, B.J. and Woollings, T. (2013b) Winter and summer northern hemisphere blocking in CMIP5 models. *Journal of Climate*, 26, 7044–7059. https://doi.org/10.1175/JCLI-D-12-00466.1.

Mattingly, K.S., Mote, T.L. and Fettweis, X. (2018) Atmospheric River impacts on Greenland ice sheet surface mass balance. *Journal of Geophysical Research-Atmospheres*, 123, 8538–8560. https://doi.org/10.1029/2018JD028714.

Mattingly, K.S., Ramseyer, C.A., Rosen, J.J., Mote, T.L. and Muthyala, R. (2016) Increasing water vapor transport to the Greenland ice sheet revealed using self-organizing maps. *Geophysical Research Letters*, 43, 9250–9258. https://doi.org/10.1002/2016GL070424.

McLeod, J.T. and Mote, T.L. (2015) Assessing the role of precursor cyclones on the formation of extreme Greenland blocking episodes and their impact on summer melting across the Greenland ice sheet. *Journal of Geophysical Research-Atmospheres*, 120, 12357–12377. https://doi.org/10.1002/2015JD023945.

McLeod, J.T. and Mote, T.L. (2016) Linking interannual variability in extreme Greenland blocking episodes to the recent increase in summer melting across the Greenland ice sheet. *International Journal of Climatology*, 36, 1484–1499. https://doi.org/10.1002/joc.4440.

Morgan, M.C. and Nielsen-Gammon, J.W. (1998) Using tropopause maps to diagnose midlatitude weather systems. *Monthly Weather Review*, 126, 2555–2579.

Nghiem, S.V., Hall, D.K., Mote, T.L., Tedesco, M., Albert, M.R., Keegan, K., Shuman, C.A., DiGirolamo, N.E. and Neumann, G. (2012) The extreme melt across the Greenland ice sheet in 2012. *Geophysical Research Letters*, 39, L20502. https://doi.org/10.1029/2012GL053611.

Pelly, J.L. and Hoskins, B.J. (2003) A new perspective on blocking. *Journal of the Atmospheric Sciences*, 60, 743–755.

Petty, G.W. (2008) *A First Course in Atmospheric Thermodynamics*. Madison WI: Sundog Publishing.

Pithan, F. and Mauritsen, T. (2014) Arctic amplification dominated by temperature feedbacks in contemporary climate models. *Nature Geoscience*, 7(3), 181–184. https://doi.org/10.1038/ngeo2071.

Ronalds, B., Barnes, E. and Hassanzadeh, P. (2018) A Barotropic mechanism for the response of jet stream variability to Arctic amplification and sea ice loss. *Journal of Climate*, 31(17), 7069–7085. https://doi.org/10.1175/JCLI-D-17-0778.1.

Serreze, M. and Francis, J. (2006) The Arctic amplification debate. *Climatic Change*, 76, 241–264. https://doi.org/10.1007/s10584-005-9017-y.

Serreze, M.C. and Barry, R.G. (2011) Processes and impacts of Arctic amplification: a research synthesis. *Global and Planetary Change*, 77(1–2), 85–96. https://doi.org/10.1016/j.gloplacha.2011.03.004.

Strong, C. and Magnusdottir, G. (2008) Tropospheric Rossby wave breaking and the NAO/NAM. *Journal of the Atmospheric Sciences*, 65(9), https://doi.org/10.1175/2008JAS2632.1.

Sutcliffe, R.C. and Forsdyke, A.G. (1950) The theory and use of upper air thickness patterns in forecasting. *Quarterly Journal of the Royal Meteorological Society*, 76(328), 189–217. https://doi.org/10.1002/qj.49707632809.

Tedesco, M., Fettweis, X., Mote, T., Wahr, J., Alexander, P., Box, J. E. and Wouters, B. (2013) Evidence and analysis of 2012 Greenland records from spaceborne observations, a regional climate model and reanalysis data. *The Cryosphere*, 7, 615–630. https://doi.org/10.5194/tc-7-615-2013.

Tedesco, M., Mote, T., Fettweis, X., Hanna, E., Jeyaratnam, J., Booth, J.F., Datta, R. and Briggs, K. (2016) Arctic cut-off high drives the poleward shift of a new Greenland melting record. *Nature Communications*, 7(1), http://dx.doi.org/10.1038/ncomms11723.

Tibaldi, S. and Molteni, F. (1990) On the operational predictability of blocking. *Tellus A: Dynamic Meteorology and Oceanography*, 42, 343–365. https://doi.org/10.3402/tellusa.v42i3.11882.

Välisuo, I., Vihma, T., Pirazzini, R. and Schäfer, M. (2018) Interannual variability of atmospheric conditions and surface melt in Greenland in 2000–2014. *Journal of Geophysical Research-Atmospheres*, 123, 10443–10463. https://doi.org/10.1029/2018JD028445.

Vavrus, S.J., Wang, F., Martin, J.E., Francis, J.A., Peings, Y. and Cattiaux, J. (2017) Changes in north American atmospheric circulation and extreme weather. *Journal of Climate*, 30, 4317–4333. https://doi.org/10.1175/JCLI-D-16-0762.1.

Wang L, Z Kuang. 2019a) . . Evidence against a general positive eddy feedback in atmospheric blocking. *arXiv preprint arXiv*: 1907.00999.

Wang, L. and Kuang, Z. (2019b) Atmospheric blocking as an evolution of Rossby wave packets. *AGUFM*, 2019, A43B–A04B.

Wilkinson, G.N. and Rogers, C.E. (1973) Symbolic descriptions of factorial models for analysis of variance. *Applied Statistics*, 22, 392–399. https://doi.org/10.2307/2346786.

Woollings, T., Hoskins, B., Blackburn, M. and Berrisford, P. (2008) A new Rossby wave–breaking interpretation of the North Atlantic oscillation. *Journal of the Atmospheric Sciences*, 65, 609–626. https://doi.org/10.1175/2007JAS2347.1.

Woollings, T., Barnes, E., Hoskins, B., Kwon, Y.O., Lee, R.W., Li, C., Madonna, E., McGraw, M., Parker, T., Rodrigues, R. and Spensberger, C. (2018) Daily to decadal modulation of jet variability. *Journal of Climate*, 31(4), 1297–1314. https://doi.org/10.1175/JCLI-D-17-0286.1.

How to cite this article: Wachowicz LJ, Preece JR, Mote TL, Barrett BS, Henderson GR. Historical trends of seasonal Greenland blocking under different blocking metrics. *Int J Climatol*. 2021;41 (Suppl. 1):E3263–E3278. https://doi.org/10.1002/joc.6923